Electronic Supplementary Information

Large second harmonic generation in penta-CdO_2 sheet exfoliated from its bulk phase

Changsheng Hou,[a] Yiheng Shen,[a] Qian Wang*[a], Y. Kawazoe,[b,c,d] and P. Jena[e]

[a] CAPT, School of Materials Science and Engineering, BKL-MEMD, Peking University, Beijing, 100871, China.

[b] New Industry Creation Hatchery Center, Tohoku University, Sendai, 980-8577, Japan;

[c] Department of Physics, Suranaree University of Technology, Nakhon Ratchasima, 30000, Thailand;

[d] Department of Physics and Nanotechnology, SRM Institute of Science and Technology, Kattankulathur, Tamil Nadu, 603203, India.

[e] Department of Physics, Virginia Commonwealth University, Richmond, VA, 23284, USA.

* Author to whom any correspondence should be addressed: qianwang2@pku.edu.cn

Table S1 The forty-five d^{10}-TM oxides from the Materials Project (MP) Database. SG represents the space group.

Formula	MP-id	SG	Formula	MP-id	SG	Formula	MP-id	SG
PdO_2	$P4_2/mnm$	1018886	CuO_2	614565	$Fmmm$	ZnO	2133	$P6_3mc$
PdO	$P4_2/mmc$	1336	CuO_2	600604	$Fmmm$	ZnO	1986	$F\bar{4}3m$
PdO_2	$Pn\bar{3}m$	10729	CuO_2	705439	$Pmmm$	ZnO_2	8484	$Pa\bar{3}$
PdO	$Fm\bar{3}m$	10728	Ag_2O	353	$Pn\bar{3}m$	ZnO	2229	$Fm\bar{3}m$
PdO	$Pm\bar{3}m$	603251	Ag_3O_4	1605	$P2_1/c$	ZnO_2	1094003	$P\bar{3}m1$
CuO	1692	$P4_2/mmc$	AgO	499	$Cccm$	CdO	1132	$Fm\bar{3}m$
Cu_2O	361	$Pn\bar{3}m$	AgO	1065190	$C2/c$	CdO_2	2310	$Pa\bar{3}$
CuO	704645	$C2/c$	AgO	1066856	$C2/c$	CdO_2	1096866	$P\bar{3}m1$
CuO	1064456	$Cccm$	Ag_2O_3	546190	$Fdd2$	CdO_2	1096876	Cm
Cu_4O_3	1478	$I4_1/amd$	AgO	1079720	$P2_1/c$	HgO	1224	$Pnma$
Cu_8O	31217	$Cmmm$	AgO	1288	$I4_1/a$	HgO	556859	$P2_1/m$

CuO	14549	$Fm\bar{3}m$	Ag_2O	7711	$P\bar{3}m1$	HgO	7826	$P3_121$
Cu_8O	704745	*Amm*2	Ag_2O_3	11872	$Pn\bar{3}m$	HgO	1077107	$P3_221$
CuO_2	1181499	*Cmcm*	AgO	8222	$F\bar{4}3m$	HgO_2	557266	*Pbca*
CuO_2	601195	*Cmcm*	Au_2O_3	27253	*Fdd*2	Hg_2O	2278	*C*2/*m*

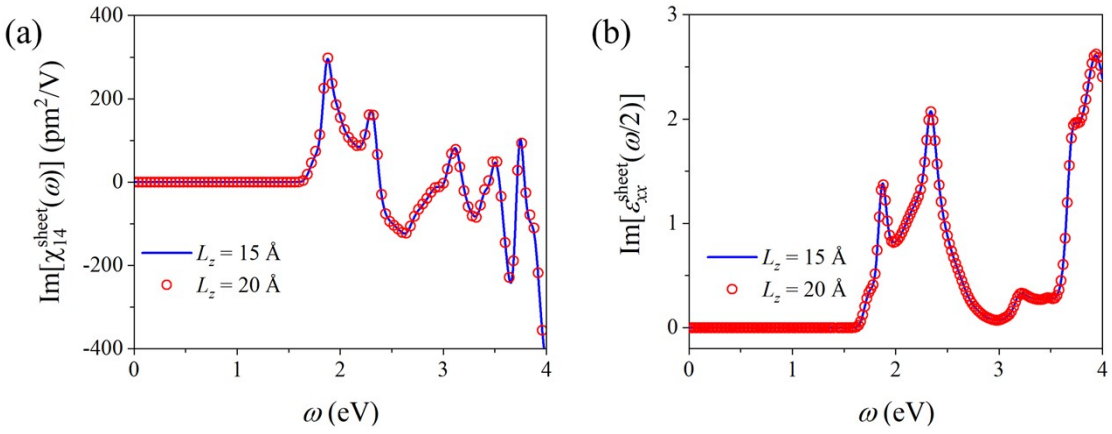

Fig. S1 Imaginary part of (a) the SHG susceptibility, and (b) the dielectric function of penta-CdO_2 obtained with different vacuum space L_z.

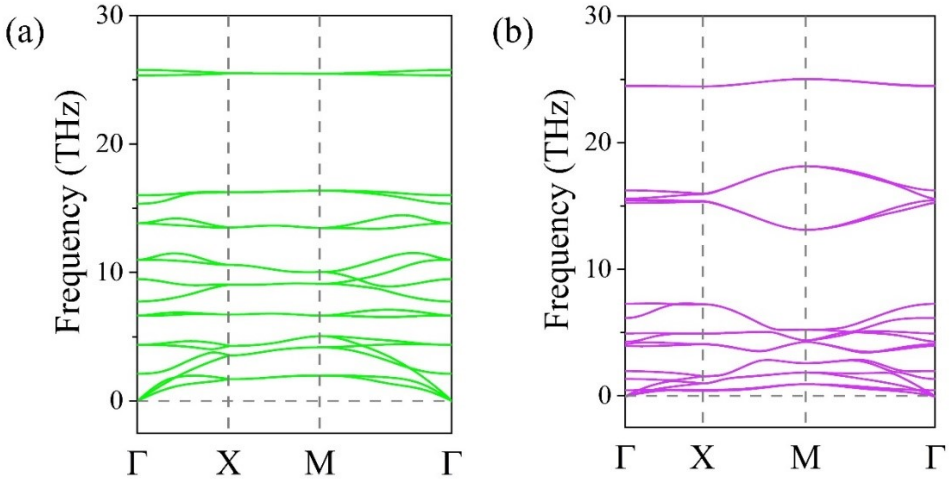

Fig. S2 Phonon spectra of (a) penta-ZnO_2 and (b) penta-HgO_2.

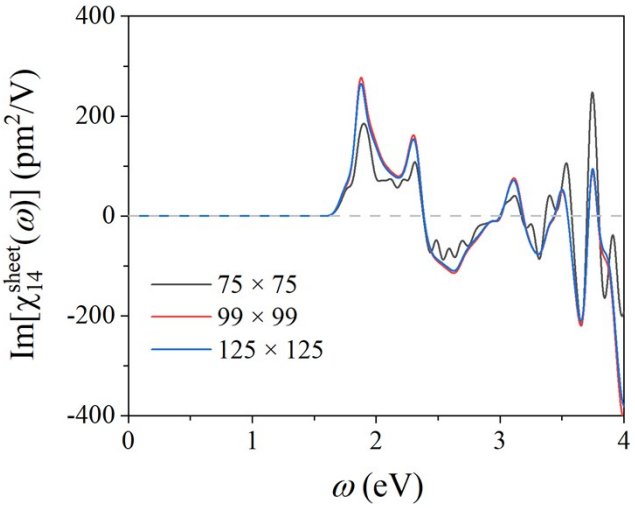

Fig. S3 Imaginary part Im[χsheet 14(ω)] of the SHG susceptibility of penta-CdO_2 obtained with different *k*-mesh.

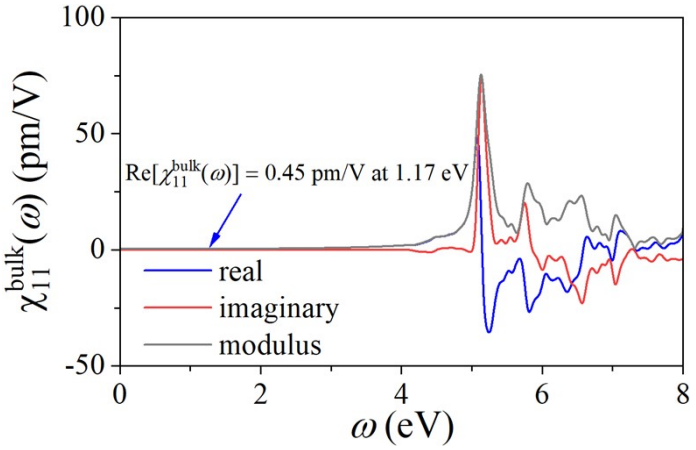

Fig. S4 SHG susceptibility χbulk 11(ω) of KBBF.

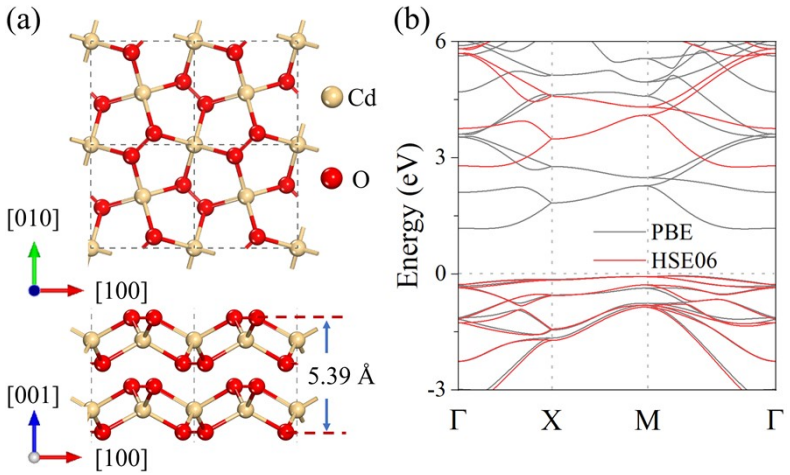

Fig. S5 (a) Top and side views of the optimized geometry, and (b) electronic band structure of bilayer penta-CdO_2.

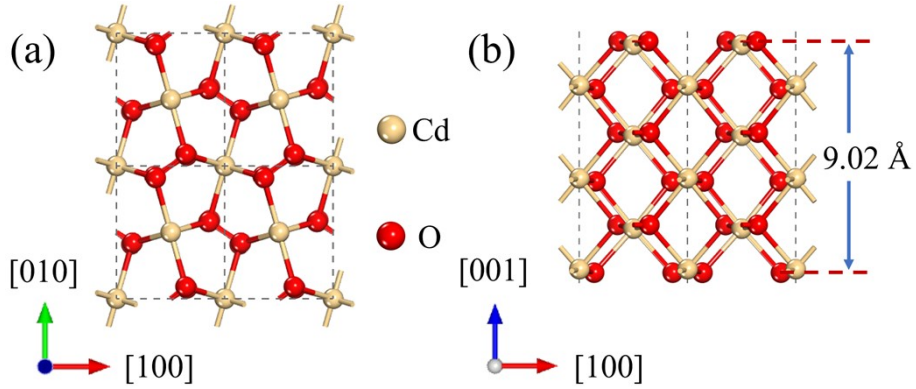

Fig. S6 (a) Top and (b) side views of the optimized geometry of trilayer penta-CdO_2.

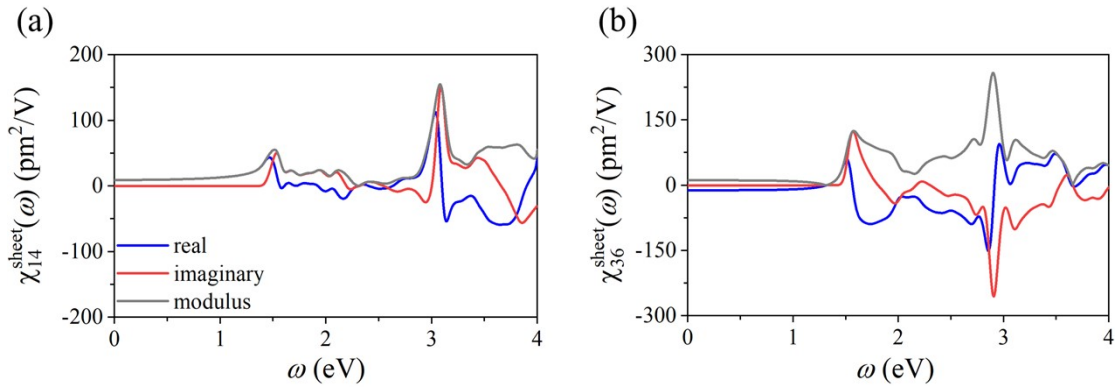

Fig. S7 SHG susceptibility of (a) χsheet 14(ω) and (b) χsheet 36(ω) of bilayer penta-CdO_2.

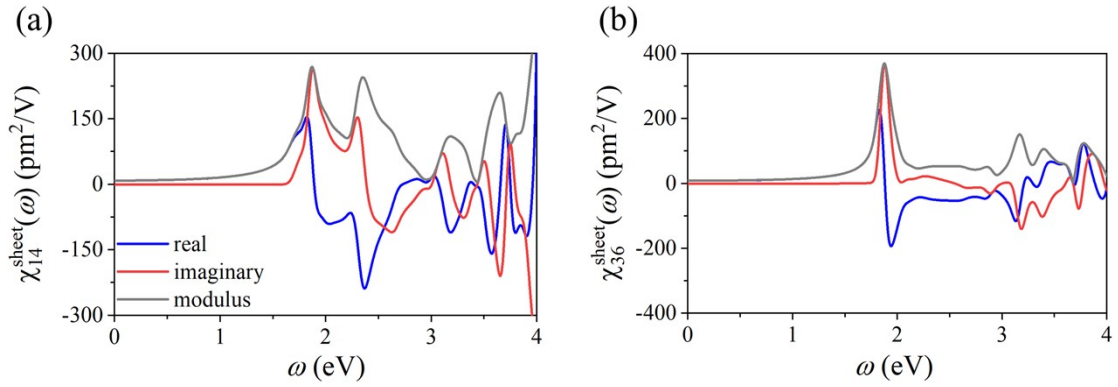

Fig. S8 SHG susceptibility (a) χsheet 14(ω) and (b) χsheet 36(ω) of penta-CdO_2.

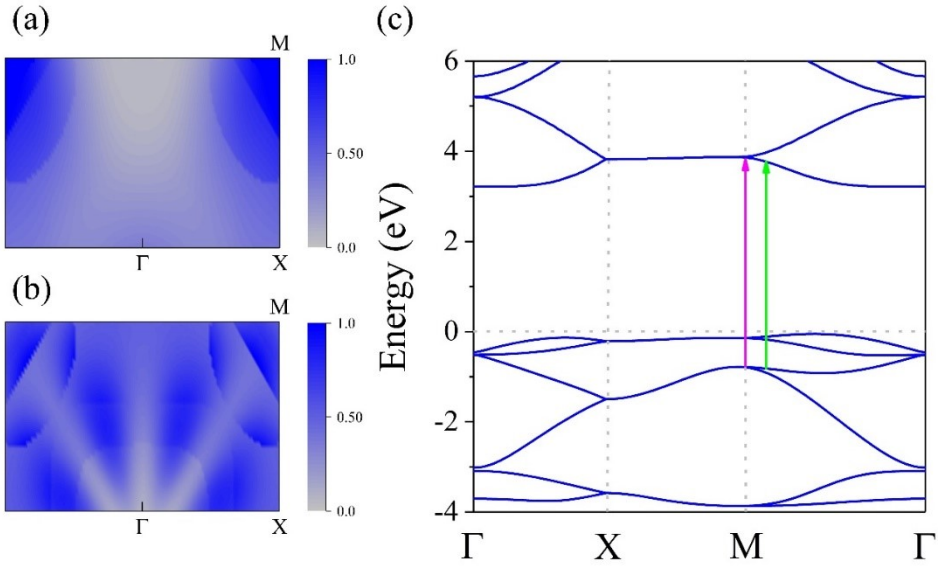

Fig. S9 Normalized k-point-dependent distributions of (a) Im[εsheet $xx(\omega/2)$] and (b) Im[εsheet $zz(\omega/2)$] at the peak value at $\omega/2$ = 1.88 eV, and (c) band structure of penta-CdO_2 at the PBE level with scissors correction.

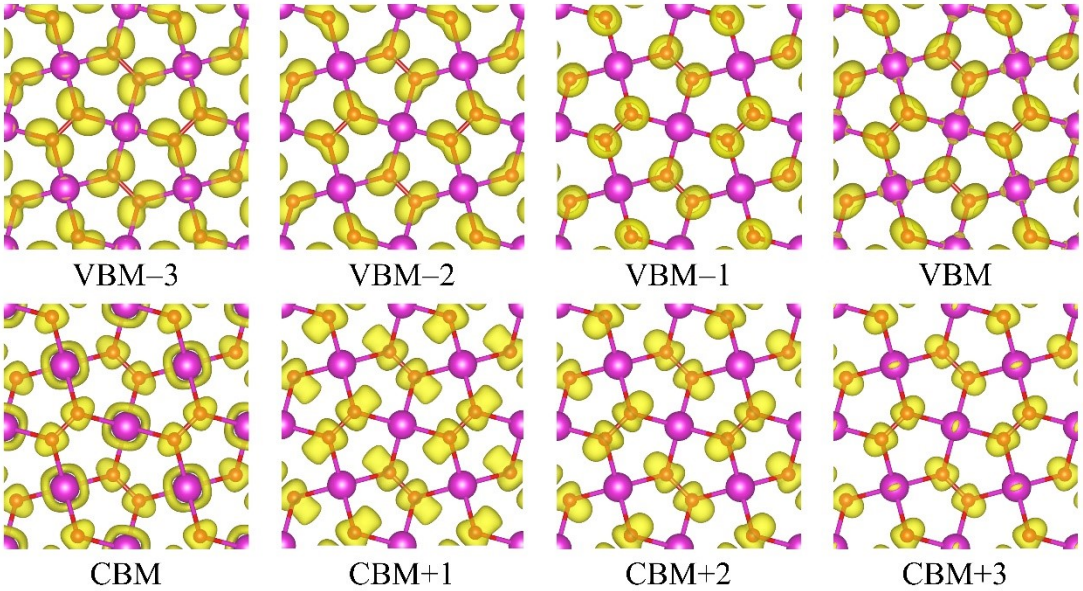

Fig. S10 Band-decomposed charge density distribution of the energy bands near the Fermi level of penta-CdO_2(isosurface values = 0.005 $Å^{-3}$).

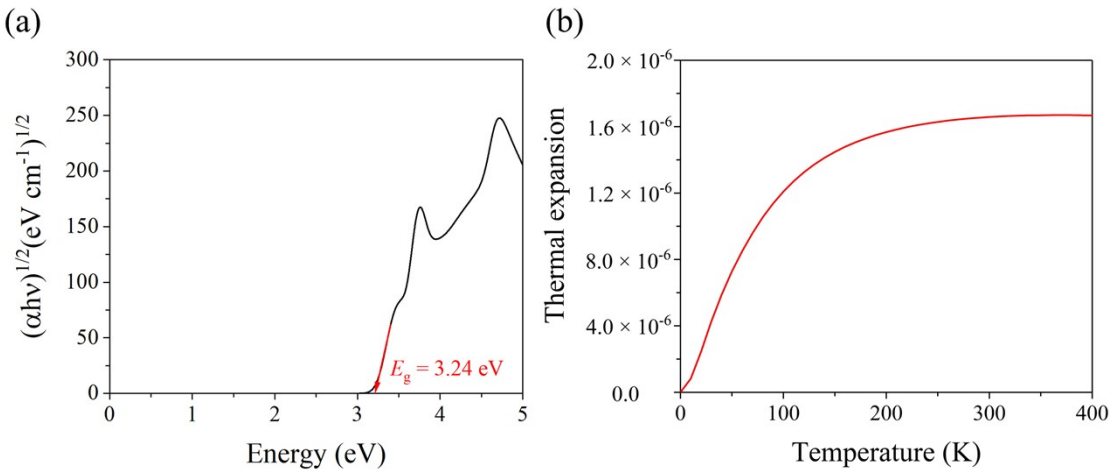

Fig. S11 (a) Optical band gap (E_g) determined from the Tauc plot, and (b) thermal expansion of penta-CdO_2.

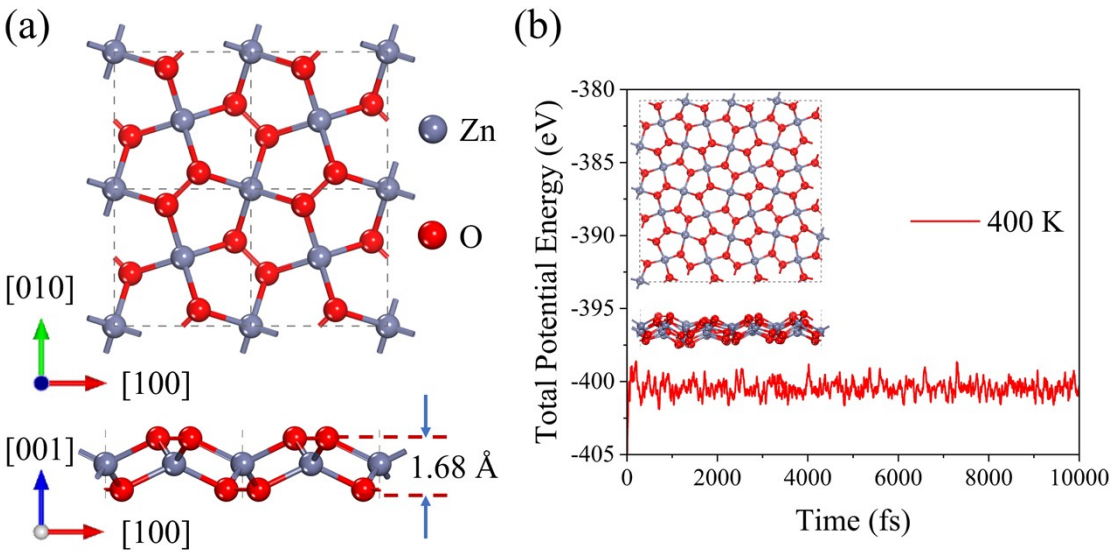

Fig. S12 (a) Top and side views of the optimized geometry of penta-ZnO_2. (b) Total potential energy fluctuation with time during the AIMD simulation at 400 K.

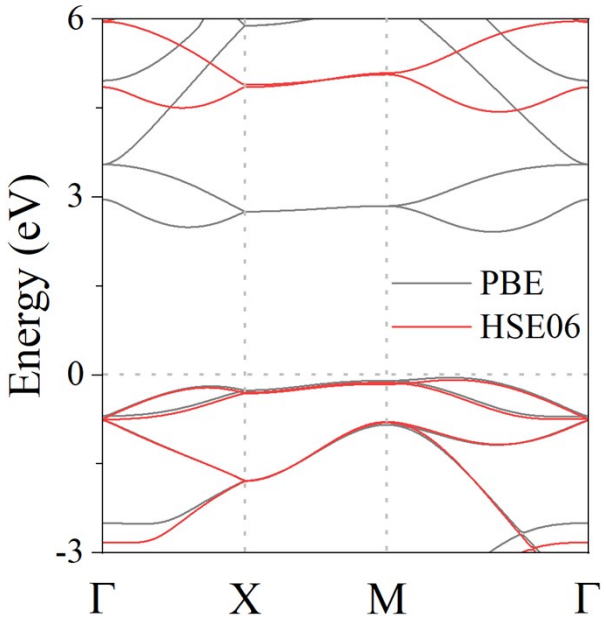

Fig. S13 Electronic band structure of penta-ZnO_2.

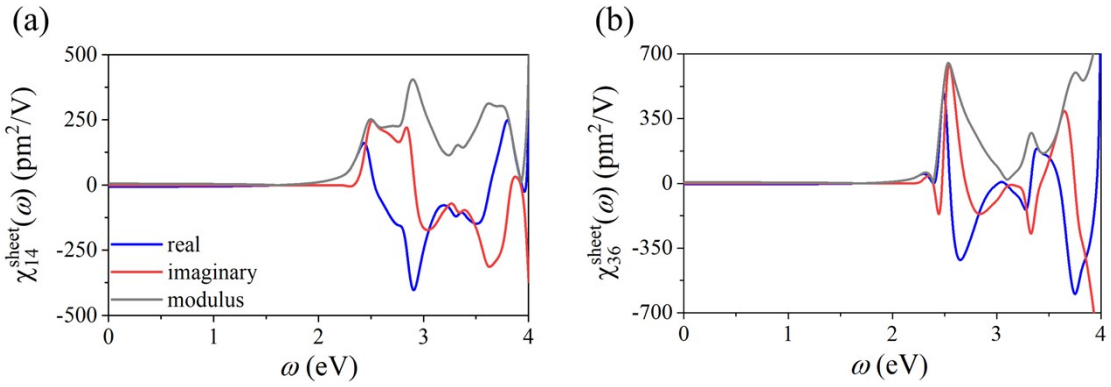

Fig. S14 SHG susceptibilities (a) χsheet 14(ω) and (b) χsheet 36(ω) of penta-ZnO_2.

We also find that another 2D d^{10}-TM oxide, penta-ZnO_2, can also exhibit large SHG response, as we expected. The fully optimized geometry of penta-ZnO_2 is presented in Fig. S12(a). Its unit cell contains two Zn and four O atoms, which occupy two nonequivalent Wyckoff positions, namely, 2b (0.500, 0.500, 0.500) and 4e (0.882, 0.618, 0.458), respectively. The lattice parameters are $a = b = 4.49$ Å. The penta-ZnO_2 sheet is also dynamically and thermally stable, as illustrated in Fig. S1(a) and Fig.

S12(b). The calculated linear elastic constants are C_{11} = 42.50 N m^{-1}, C_{12} = 3.00 N m^{-1}, and C_{66} = 22.56 N m^{-1}, which meet the requirements of Born-Huang criteria ($C_{11} > 0$, $C_{11} > C_{12}$ and $C_{66} > 0$),[50] confirming that penta-ZnO_2 is mechanically stable. The band structures of penta-ZnO_2 at the HSE06 level and PBE level are given in Fig. S13, which show that penta-ZnO_2 is also semiconducting with an indirect band gap of 2.46 eV at the PBE level, and 4.52 eV at the HSE06 level, larger than the corresponding values of 1.45 and 3.28 eV, respectively, for penta-CdO_2. We further explore its potential for SHG performance because of the non-centrosymmetric and non-metallic features of penta-ZnO_2. We find that penta-ZnO_2 possesses strong in-plane and out-of-plane SHG response with large static SHG susceptibilities of χsheet 14(0) = χsheet 25(0) = χsheet 36(0) = –5.60 pm^2/V. We further calculate the frequency-dependent SHG susceptibility of penta-ZnO_2, especially consider its imaginary part (Im[χsheet $abc(\omega)$]). The real parts, imaginary parts, and modulus of different nonzero independent SHG tensor components are plotted in Fig. S14. One can see that the Im[χsheet 14(ω)] and Im[χsheet 36(ω)] of penta-ZnO_2 have the most significant peak values of 236.85 pm^2/V and 639.56 pm^2/V at 2.54 eV, respectively. The most significant peak value of Im[χsheet $abc(\omega)$] in penta-CdO_2 is at a lower energy range due to its smaller band gap of 3.28 eV at the HSE06 level compared with that of penta-ZnO_2, leading to a larger SHG response in penta-CdO_2.